Journal of Membrane Science 596 (2020) 117689

Contents lists available at ScienceDirect

Journal of Membrane Science

journal homepage: http://www.elsevier.com/locate/memsci

In-situ linker doping as an effective means to tune zeolitic-imidazolate framework-8 (ZIF-8) fillers in mixed-matrix membranes for propylene/propane separation

Sunghwan Park [a], Hae-Kwon Jeong [a,b,*]

[a] Artie McFerrin Department of Chemical Engineering, Texas A&M University, 3122 TAMU, College Station, TX, 77843-3122, United States
[b] Department of Materials Science and Engineering, Texas A&M University, 3122 TAMU, College Station, TX, 77843-3122, United States

ARTICLE INFO

Keywords:
Mixed-matrix membrane
In-situ growth
Linker-doping
Zeolitic-imidazolate framework
Propylene/propane separation

ABSTRACT

Zeolitic-imidazole framework-8 (ZIF-8) has been extensively studied as a molecular sieving filler in mixed-matrix membranes (MMMs) for propylene/propane (C3) separation. The C3 separation performance of ZIF-8-containing MMMs has yet to meet the commercial viability criteria. Recently, doping or mixing linkers in ZIF-8 framework has been found effective in tuning the molecular sieving properties of ZIF-8. Herein, we attempted to tune the molecular sieving properties of ZIF-8 fillers in MMMs by doping with 2-ethylimidazole (eIm) linkers in order to improve their C3 separation performance. MMMs were prepared by *in-situ* forming eIm-doped ZIF-8 fillers in polyimide using our recently reported polymer-modification-enabled *in-situ* MOF formation (PMMOF) process. As eIm linkers were doped into ZIF-8 filler crystals, the propylene/propane separation factor of the resulting MMMs was dramatically enhanced. Lastly, doped-linker ZIF-8 based mixed-matrix hollow fiber membranes were successfully prepared, demonstrating potential of their scalable practical applications.

1. Introduction

Propylene/propane (C3) separation is one of the most energy-intensive processes in the petrochemical industry [1]. Membrane-based C3 separation requires only ~ 10% energy of the conventional thermally-driven distillation process [2]. In particular, mixed-matrix membranes (MMMs), consisting of a continuous polymer phase and a dispersed molecular sieve phase, have been considered as a promising next-generation membrane concept by combining the advantages of both polymer and molecular sieve membranes [3].

Among several promising fillers for propylene-selective MMMs, zeolitic-imidazole framework-8 (ZIF-8) is one of the most promising and investigated fillers due to its effective aperture size (i.e., 4.0–4.2 Å) [4]. ZIF-8 consists of Zn^{2+} nodes bridged by flexible 2-methylimidazole (mIm) linkers, forming sodalite (SOD) topology. Among a number of ZIF-8 containing MMMs, however, there are only a handful of MMMs reported for C3 separation. Koros et al. [5,6] successfully demonstrated the applicability of MMMs for C3 separation by preparing 4,4′-(hexafluoroisopropylidene) diphthalic anhydride-2,4,6-trimethyl-1, 3-diaminobenzene (6FDA-DAM)/ZIF-8 MMMs in the form of both flat sheet membranes and hollow fiber membranes. The MMMs showed improved C3 separation performances attributed to the well-matching of the polymer and ZIF-8 [3]. Nevertheless, even with ZIF-8 loading as high as 48 wt%, the 6FDA-DAM/ZIF-8 MMMs fell short of meeting the commercial viability criteria (i.e., minimum C_3H_6 permeability of 1 Barrer and selectivity of 35) [7]. It is noted that the intrinsic propylene and propane permeabilities of ZIF-8 are reported ~ 210 and ~2.5 Barrer, respectively [4]. As such, the minimum ZIF-8 loading in 6FDA-DAM required to meet the commercial viability criteria is estimated ~ 60 wt% based on Maxwell model. This strongly suggests the need to find better molecular sieving fillers and/or to further improve composite microstructures by developing better processing methods.

In general, it is quite time-consuming, expensive, and often impossible to find or synthesize more propylene-selective molecular sieving fillers including new ZIFs than ZIF-8 [8]. A more rational strategy is to fine-tune the effective aperture size of ZIF-8 by introducing additional metal centers and/or linkers (known as hybrid ZIFs) [9,10]. For example, Jeong et al. [10] showed mixed-metal CoZn-ZIF-8 membranes exhibited enhanced C3 separation performance than mono-metallic ZIF-8 membranes. Computational studies by Krokidas et al. [11,12] revealed that mixing cobalt and zinc metal centers led to shortening of the metal-linker bond length and to increasing of the bond stiffness

* Corresponding author. Artie McFerrin Department of Chemical Engineering, United States.
E-mail address: hjeong7@tamu.edu (H.-K. Jeong).

https://doi.org/10.1016/j.memsci.2019.117689
Received 17 October 2019; Received in revised form 22 November 2019; Accepted 25 November 2019
Available online 29 November 2019

between metal centers and mIm linkers, consequently reducing the effective aperture size of ZIF-8 framework. Nair et al. [9,13] first reported mixed-linker ZIFs, ZIF-8-90 and ZIF-7-8, via *de novo* synthesis and showed continuous control of effective aperture size and polarity [13] and drastic enhancement of their molecular sieving properties for light gas separations [14–17]. Very recently, Jeong et al. [18] reported doped-linker ZIF-8 showing tunable molecular sieving properties. Unlike mixed-linker ZIF-8 where both linkers are capable of forming isostructures of SOD-ZIF-8, doped-linker ZIF-8 has an additional linker (i.e., dopant linker) which alone is not capable of forming SOD-ZIF-8 structures. ZIF-8 particles doped with 2-ethylimidazolate (eIm) showed restricted metal-linker flexibility, implying reduced effective aperture size.

Besides, microstructures of MMMs (i.e., interfacial structures and filler dispersion) play critical roles for their gas separation performances [19–21]. Conventional physical blending methods for MMM preparation pose several challenges that often lead to poor microstructures including interfacial void formation and agglomeration of filler nanoparticles [22]. Recently, we reported the polymer-modification-enabled *in-situ* metal-organic framework formation (PMMOF) process as a scalable MMM fabrication strategy [23]. Since MOF filler nanoparticles formed *in-situ* inside a modified polyimide, the PMMOF was found highly effective in addressing some of the challenges of conventional MMM processing. The resulting 6FDA-DAM/ZIF-8 MMMs showed much higher C3 separation than conventionally-prepared MMMs due to the better adhesion and dispersion of ZIF-8 as well as polymer densification. Moreover, the PMMOF decouples membrane fabrication from filler incorporation process, thereby rendering it commercially more attractive.

Here, we report eIm-doped ZIF-8-containing MMMs prepared by *in-situ* forming doped ZIF-8 fillers inside 6FDA-DAM polymer by PMMOF. *In-situ* grown eIm-doped ZIF-8 nanoparticles inside the polymer were characterized and compared with corresponding eIm-doped ZIF-8 particles that were solution precipitated. Binary propylene/propane separation performance of the 6FDA-DAM/eIm-doped ZIF-8 MMMs was measured and compared with that of conventionally prepared MMMs. Lastly, eIm-doped ZIF-8-based mixed-matrix hollow fiber membranes were prepared by PMMOF and their C3 separation performance was examined.

2. Experimental

2.1. Materials

6FDA-DAM (Mw: 148 k, PDI: 2.14) was purchased from Akron Polymer Systems Inc. Sodium formate (HCOONa, ≥ 99%, Sigma Aldrich), zinc nitrate hexahydrate (Zn(NO3)2·6H2O, 98%, Sigma Aldrich), 2-methyimidazole (mIm) (C4H6N2, ≥98%, Sigma Aldrich), and 2-ethylimidaole (eIm) (C5H8N2, ≥98%, Sigma Aldrich) were used. N,N-dimethylformamide (DMF) (C3H7NO, > 99.8%, Alfa Aesar), ethyl acetate (EtOAc) (C4H8O2, ≥99.5%, VWR International), and methanol (CH3OH, > 99.8%, Alfa Aesar) were used as a solvent. All chemicals were used as received.

2.2. Synthesis of eIm-doped ZIF-8 particles by solution precipitation

A metal solution and a ligand solution were prepared separately. The metal solution was prepared by dissolving 2.5 mmol of zinc nitrate hexahydrate in 15 ml methanol. The ligand solution was made by dissolving total 25 mmol of ligands in 15 ml methanol. The ligand solution was added to the metal solution and mixed for about 1 min. The ligand composition of each linker solution was as follows; 1) 25 mmol of mIm, 2) 20 mmol of mIm and 5 mmol of eIm, 3) 15 mmol of mIm and 10 mmol of eIm, 4) 10 mmol of mIm and 15 mmol of eIm, 5) 5 mmol of mIm and 25 mmol of eIm. The crystallization was carried out at 40 °C for 2 h in a Teflon-lined stainless-steel autoclave. It is noted that the autoclave was used for consistency since the crystallization temperature was varied and optimized. The powder samples were collected by centrifugation with 8000 RPM for 20 min. The samples were re-dispersed in methanol by sonication for 30 min and then centrifuged again at the same conditions. The purification steps were repeated two more times to achieve high purity particles. After the purification, the powders were dried at 60 °C for overnight. The samples were denoted as eImx-ZIF-8 where the subscript represents the eIm fraction of the total linkers present in a linker treatment solution, ranging from 0.2–0.8.

2.3. Preparation of 6FDA-DAM/eIm-doped ZIF-8 MMMs by PMMOF

Thin 6FDA-DAM polymer films were prepared on porous α-alumina disks (diameter of 2.2 cm) made according to a previous recipe described elsewhere [14]. In a typical preparation, a polymer solution was prepared by dissolving 0.25 g of 6FDA-DAM in 12.25 g of DMF. 2.4 ml of the polymer solution was slowly dropped onto the polished side of a porous α-alumina disk. Immediately, the sample was placed in a vacuum oven pre-heated at 150 °C and dried for 1 day, forming a polymer film with a thickness of 8.0 ± 1.5 μm on the α-alumina disk. PMMOF process was then applied to the polymer film as detailed in our recent report [23]. The hydrolysis of the polymer film was carried out in a sodium formate solution (100 mmol of sodium formate in 30 ml of D.I. water). The polymer film was vertically located in a custom-made Teflon holder and then placed in a Teflon-lined autoclave containing the sodium formate solution. The hydrolysis was conducted at 120 °C for 5 h. After washed with deionized (DI) water overnight using a lab shaker, the sample was subjected to an ion exchange by immersing it in an ion exchange solution (20 mmol of zinc nitrate hexahydrate in 30 ml of DI water) for 3 h. After briefly washed with methanol, the ion-exchanged sample was put into a ligand solution prepared by dissolving 25 mmol of linker mixtures in total in 30 ml of methanol with varying eIm compositions; 0%, 20%, 40%, 60%, and 80%. A ligand treatment was executed in a Teflon-lined autoclave at 40 °C for 2 h, followed by washing with methanol overnight. Lastly, the sample was thermally imidized at 220 °C for 3 h in a pre-heated convection oven. Hereafter, the eIm-doped ZIF-8 containing MMMs were named as PI/eImx-ZIF-8 (x = 0.2, 0.4, 0.6, or 0.8) where the subscript represents the eIm fraction of total linkers in the linker treatment solution.

2.4. Preparation of PI/eIm-doped ZIF-8 MMMs by physical blending

For comparison, MMMs were also prepared on porous α-alumina disks using conventional physical blending. Preformed eIm-doped ZIF-8 particles of proper amounts (i.e., 4.8 mg of ZIF-8, 4.6 mg of $eIm_{0.2}$-ZIF-8, 3.9 mg of $eIm_{0.4}$-ZIF-8, 2.8 mg of $eIm_{0.6}$-ZIF-8, 1.2 mg of $eIm_{0.8}$-ZIF-8) were fully dispersed in 0.98 g of DMF under sonication for 30 min. 20 mg of 6FDA-DAM was then added to an eIm-doped ZIF-8 suspension, followed by further sonication for 30 min. 2.4 ml of the prepared polymer/filler solution was slowly dropped onto an α-alumina disk. Immediately after, the sample was placed in a pre-heated oven at 150 °C and dried for 1 day at the same temperature under vacuum.

2.5. Coating of 6FDA-DAM on polymer hollow fibers

Polyethersulfone (PES) microfiltration hollow fibers (surface pore size of ~200 nm, Repligen Co.) were coated with thin 6FDA-DAM layers by dip-coating inside a glove bag saturated with EtOAc. A 6FDA-DAM solution was prepared by dissolving 0.50 g of 6FDA-DAM in 12.0 g of EtOAc. An as-purchased PES hollow fiber was dipped in the prepared polymer dope solution. Immediately after, the fiber was taken out and dried vertically in the glove bag for 7 h. The resulting 6FDA-DAM coated PES hollow fiber was dried at room temperature for 1 h and then at 60 °C overnight in a convection oven.

2.6. Characterizations

Scanning electron microscope (SEM) images were taken using a JEOL JSM-7500F at an acceleration voltage of 5 keV with 15 mm working distance. Transmission electron microscope (TEM) images were collected using a FEI Tecnai FE-TEM under cryogenic conditions using microtomed samples. Powder X-ray diffraction (PXRD) was collected using a Rigaku Miniflex II at a 2 θ range of 5–40° with Cu-Kα radiation (λ = 1.5406 Å). Nitrogen adsorption isotherms were obtained using ASAP 2010 (Micromeritics) at 77 K after degassing samples at 150 °C under vacuum for 24 h. Solution proton nuclear magnetic resonance (1H NMR) spectra were obtained using a Bruker Avance III (500 MHz system). Solution NMR samples were prepared by dissolving ZIF samples in 550 μL of deuterated acetic acid-d4. Fourier transform infrared (FT-IR) spectra were measured by a Nicolet iS5 spectrophotometer (Thermo Scientific) equipped with an attenuated total reflectance (ATR, iD7) accessory. X-ray photoelectron spectroscopy (XPS) was performed using an Omicron ESCA+ with Mg X-ray source at 300 W. Thermogravimetric analysis (TGA, Q50 TA instruments) was carried out at a temperature range from 25 °C to 700 °C at heating rate of 10 °C/min.

2.7. Gas permeation measurements

Gas permeation characteristics of membranes were measured by the Wicke-Kallenbach technique using equimolar binary C_3H_6 and C_3H_8 gas mixture at room temperature under atmospheric pressure. Feed gas was provided at 20 cm^3 min^{-1}, while the permeate side was swept by argon gas with the flow rate of 20 cm^3 min^{-1}. A steady-state of gas permeation was declared when the deviation of measured gas permeance was less than 1% with 30 min interval. The permeated gas compositions were determined using a gas chromatography (GC 7890A, Agilent) equipped with a flame ionized detector (FID) and a HP-plot Q column.

3. Results & discussion

3.1. Characterizations of MMMs containing 2-ethylimidazole (eIm)-doped ZIF-8

MMMs containing 2-ethylimidazole (eIm)-doped ZIF-8 (i.e., Zn $(mIm)_{2-x}(eIm)_x$) were prepared by *in-situ* growth of ZIFs in 6FDA-DAM polyimide (PI) using PMMOF. As illustrated in Fig. S1, PMMOF includes four steps: hydrolysis of PI, ion exchange, ligand treatment, and imidization. As detailed in our recent report [23], each step was described and characterization results were presented in the Supporting Information (Figs. S2–3). Fig. 1a presents the XRD patterns of the resulting PI/eIm-doped ZIF-8 MMMs, showing SOD-ZIF-8 phases regardless of the eIm percentages [18]. As shown in the scanning electron micrographs of MMMs in Fig. 1b–f, many particles were found on the surface. To verify the presence of ZIF crystals inside the polymer, the surface-bound ZIF crystals were removed by wiping with a dilute nitric acid (Fig. S4) [23]. While surface-bound ZIF crystals were completely removed (Figs. S4b–f), the X-ray diffraction patterns of the MMMs were still observed (Fig. S4a), though the intensities were slightly decreased. This confirmed that the substantial fraction of ZIF crystals were *in-situ* formed inside the polymer.

As the eIm content increased, the crystal size of surface-bounded eIm-doped ZIF-8 increased from ~100 nm to ~500 nm (Fig. 1b–f), following the same trend as solvothermally synthesized eIm-doped ZIF-8 (Figs. S5–7) [18]. Since the pKa value of eIm (8.00) is higher than that of mIm (7.86) [24], the higher pKa might decrease the crystal growth rate, forming larger crystals [25]. In stark contrast, the size of eIm-doped ZIF-8 grown inside the polymer seemed to be not affected by changing eIm-doping compositions. Fig. 2 presents cross-sectional transmission electron micrographs and electron diffraction patters of the membranes. As indicated by arrows in Fig. 2 a1-d1, spherical shaped eIm-doped ZIF-8

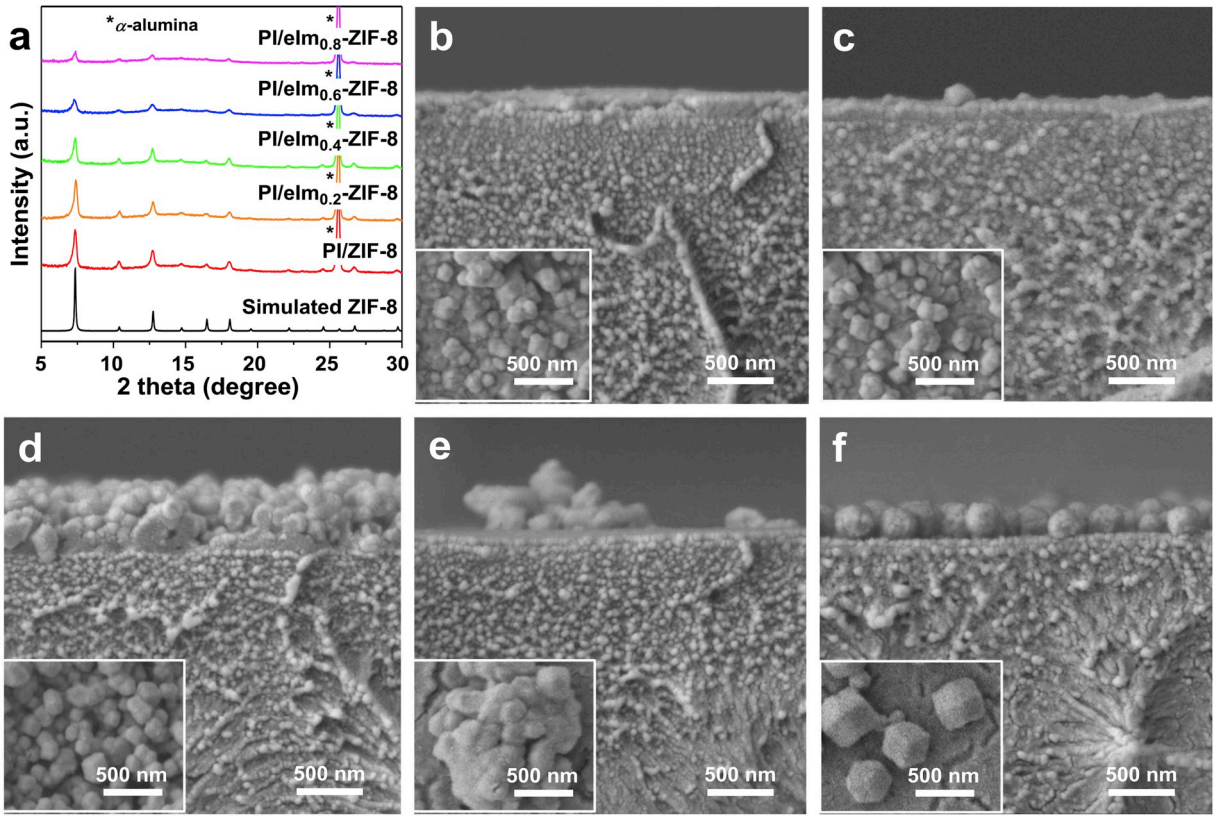

Fig. 1. a XRD patterns of as-prepared PI/ZIF-8 and PI/eIm-doped ZIF-8 MMMs by PMMOF. **b-f** SEM images of as-prepared MMMs by PMMOF; PI/ZIF-8 (b), PI/$eim_{0.2}$-ZIF-8 (c), PI/$eim_{0.4}$-ZIF-8 (d), PI/$eim_{0.6}$-ZIF-8 (e), and PI/$eim_{0.8}$-ZIF-8 (f). The inset images on the bottom left are top views of the corresponding samples.

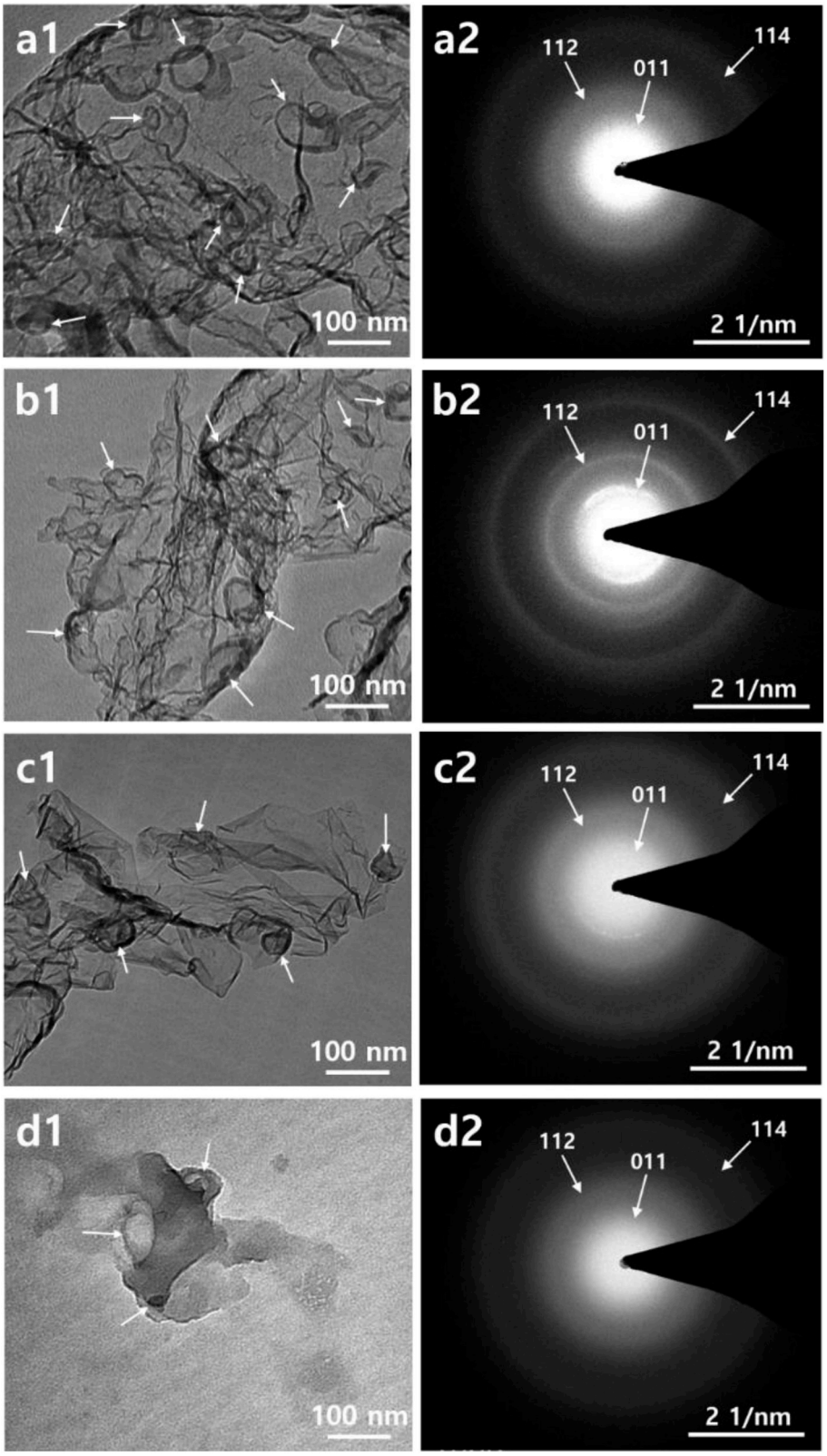

Fig. 2. a1-d1 TEM images of PI/eIm-doped ZIF-8 MMMs (left column) and **a2-d2** their corresponding SAED patterns (right column). PI/eIm$_{0.2}$-ZIF-8 (a). PI/eIm$_{0.4}$-ZIF-8 (b). PI/eIm$_{0.6}$-ZIF-8 (c). PI/eIm$_{0.8}$-ZIF-8 (d).

particles of sub-100 nm in size were observed. Interestingly, a poorly defined phase was observed as well (Fig. 2 a1-d1). Considering its morphology, the unknown phase seems lacking crystallinity, which might be similar to the so called not well-crystallized ZIF deposit formed in confined spaces reported by Ma and Tsapatsis et al. [26] This is possibly due to the *in-situ* nucleation and growth of eIm-doped ZIF-8 crystals in confined spaces (i.e., polymer free volume) [23]. It is reminded that a larger filler size fundamentally limits the preparation of

ultra-thin active layers (i.e., <1 μm) in MMMs [6]. However, the sub-100 nm size of *in-situ* formed eIm-doped ZIF-8 fillers, independent of eIm-doping compositions, is highly desirable to achieve ultra-thin active layers.

^{1}H NMR analysis was performed to determine the actual compositions of eIm linkers doped in ZIF-8 fillers inside the polymer. Surface-bound crystals were completely removed from the samples in order to measure only those embedded inside the polymer. Fig. 3 shows ^{1}H NMR spectra of the samples with various eIm percentages in the ligand treatment solutions. Based on the NMR analysis, the percentages of eIm linkers actually doped in ZIF-8 were estimated approximately 7, 16, 31, and 48 mol% with 20, 40, 60, and 80 mol% in the linker treatment solutions, respectively. At first, the lower eIm content in ZIF-8 than in precursor solutions was attributed due to the different diffusion rates of linkers in the polymer, which can be varied by size, solvent, affinity with polymer, and others. The eIm compositions in doped-ZIF-8 were, however, comparable with those of solution precipitated ones; approximately 6, 15, 28, and 48 mol% (Fig. S7). This strongly indicates that the doping of eIm was not significantly affected by diffusion of linkers under the current conditions. Instead, the doping was likely determined by the fact that mIm was more favorably incorporated to ZIF-8 than the bulkier eIm [18]. Nevertheless, the more eIm present in the precursor solutions, the more eIm doped in ZIF-8 frameworks.

It is important to quantify the filler loadings in MMMs to investigate the effect of fillers on gas separations [3,5]. The loadings of ZIF-8 and eIm-doped ZIF-8 in MMMs were determined by thermal oxidization after eliminating surface-bound ZIFs by the acid treatment (Fig. S8 and Table S1). Interestingly, the filler content in MMMs gradually decreased as the content of eIm dopants increased (Fig. 4). This is further confirmed by a gradual decrease in the XRD intensity of MMMs as the eIm content increased regardless of the presence of surface-bound eIm-doped ZIF-8 crystals (Fig. S9). The decrease in eIm-doped ZIF-8 loadings with increasing eIm fractions appeared following the same trend as the yields of doped ZIF-8 synthesized in solutions (Fig. 4), strongly suggesting the presence of a close correlation between the filler contents in MMMs and the yield of solution-precipitated doped crystals. In other words, the filler contents in MMMs by PMMOF can be deduced by the yield of solution-precipitated doped fillers.

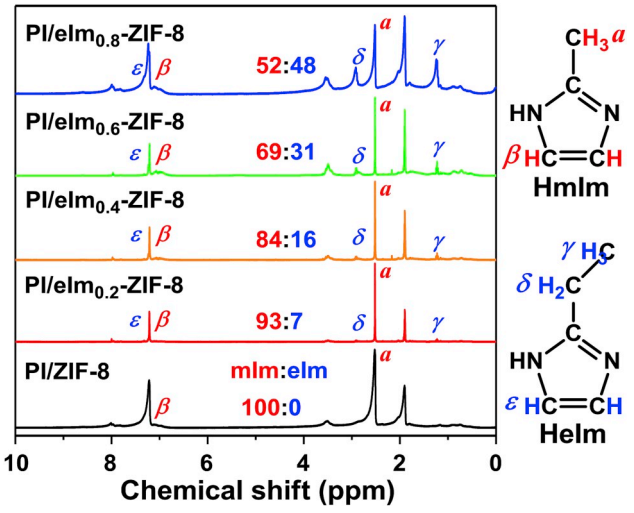

Fig. 3. ^{1}H NMR spectra of PI/ZIF-8 and PI/eIm-doped ZIF-8 MMMs by PMMOF. The ratios between mIm and eIm incorporated in the frameworks were noted and determined based on the following formula: eIm% = $(A_\gamma/3)/[(A_\beta + A_\varepsilon)/2]$ where A represents peak area.

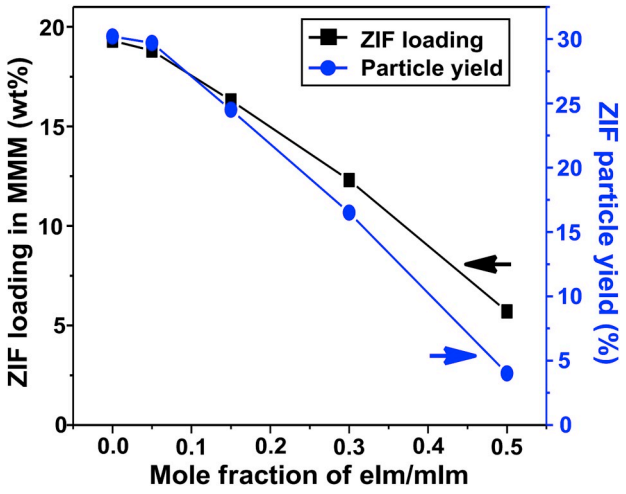

Fig. 4. Comparison of eIm-doped ZIF-8 loadings in MMMs by PMMOF and yields of solution-precipitated eIm-doped ZIF-8 crystals.

3.2. Propylene/propane separation performance of eIm-doped ZIF-8-based MMMs

The C3 separation performances of the PI/eIm-doped ZIF-8 MMMs are presented in Fig. 5 and Table S2. Despite the relatively lower loadings of eIm-doped ZIF-8 (12.3–18.8 wt%) in MMMs than that of ZIF-8 (19.3 wt%) (Table S1), the PI/eIm-doped ZIF-8 MMMs exhibited improved C3 separation performances as compared to the PI/ZIF-8 (Fig. 5). The MMMs containing eIm-doped ZIF-8 fillers with the relatively low eIm-dopant content (i.e., PI/eIm$_{0.2}$-ZIF-8) exhibited the C_3H_6 permeability ~ 62% higher than the PI/ZIF-8 with a similar separation factor (Fig. 5 and Table S2). On the contrast, the PI/eIm$_{0.6}$-ZIF-8 showed the opposite trend that there was a slight decrease in the C_3H_6 permeability by ~18% with a significantly enhanced separation factor (~111%), meeting the so called commercially-viable performance criteria [7,27]. (Fig. 5 and Table S2). It is noted that most of the previous studies on MMMs for C3 separation failed to significantly improve separation factors except a few [5,28–36]. In the case of the PI/eIm$_{0.4}$--ZIF-8, the C3 separation performance was in between those of the PI/eIm$_{0.2}$-ZIF-8 and the PI/eIm$_{0.6}$-ZIF-8; both the C_3H_6 permeability (~16%) and the C_3H_6/C_3H_8 separation factor (~75%) were higher than

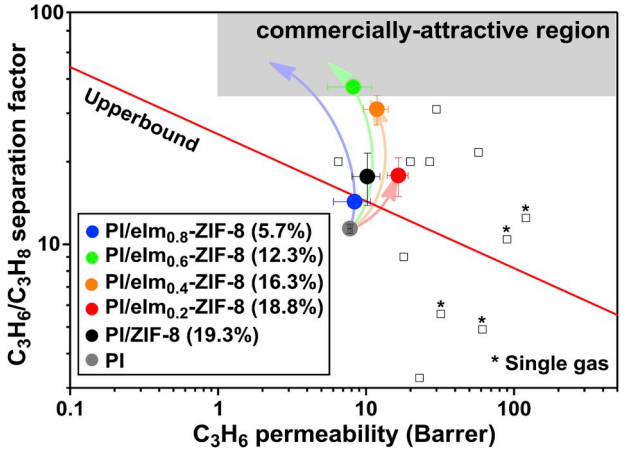

Fig. 5. C_3H_6/C_3H_8 upper bound plot of PI/ZIF-8 and PI/eIm-doped ZIF-8 MMMs prepared by PMMOF (solid circle) and the MMM data in literatures (open rectangular).[5, 28–36] Note: the arrows are arbitrarily drawn for illustration purpose to indicate the hypothetical separation performance improvement of PI/eIm-doped ZIF-8 MMMs when eIm-doped ZIF-8 loading increases up to ~20 wt%.

those of the PI/ZIF-8 (Fig. 5 and Table S2). The PI/eIm$_{0.8}$-ZIF-8 showed the separation performance lower than the PI/ZIF-8 (Figs. 4 and 5) possibly due to the ~ 3-fold lower ZIF contents in polymer (5.7 wt%). In light of this, the higher loading of eIm-doped ZIF-8 in the polymer would lead to further improved C3 separation performances of MMMs as drawn in the arrows in Fig. 5.

Interestingly, the enhanced separation factor of PI/eIm-doped ZIF-8 MMMs with increasing eIm-dopant contents seems to deviate from eIm-doped ZIF-8 polycrystalline membranes recently reported by our group [18]. For the polycrystalline membranes, a systematic increase in the permeance and a decrease in the separation factors were observed as the eIm dopant content increased. This opposite trend might be attributed to the relatively low eIm doping (up to 2.5% eIm in the framework) in the case of the polycrystalline membranes [18], since there exists a threshold concentration of doped linker for tuning of effective aperture size [37]. More importantly, unlike eIm-doped ZIF-8 polycrystalline membranes, the flexibility of ligands is likely restricted by a strong interaction with the surrounding polymer, thereby reducing the flip-flopping motion of eIm-doped ZIF-8 in MMMs [38].

As such, we attributed the systematic enhancement in the C3 separation performances of eIm-doped ZIF-8 containing MMMs to the effective tuning of ZIF-8 apertures resulting from relatively high eIm doping [18] and restricted flip-flopping motion of linkers [38]. To further investigate, N_2 adsorption studies were conducted on eIm-doped ZIF-8 crystals that were solvothermally synthesized (Fig. 6). Table S3 summarizes the surface areas and the pore volumes of the eIm-doped ZIF-8 particles, which are consistent with the previous report [18]. As shown in Fig. 6, there were two threshold pressures of sudden increases in N_2 adsorption, known as "gate-opening" [39]. The second gate-opening pressure moved to the higher relative pressure with increasing eIm contents and eventually disappeared for the doped ZIF-8 with eIm content greater than 31 mol% (eIm$_{0.6}$-ZIF-8). Since the gate-opening of ZIFs is caused by the reorientation of flexible organic linkers [16,39], this shift in the gate-opening pressure toward higher relative pressure strongly suggests that the flexibility of ZIF-8 was restricted by incorporation of eIm linkers. Furthermore, the ATR-FTIR spectra shown in Fig. S10 clearly exhibit blue-shifts of the Zn–N vibration of eIm-doped ZIF-8 at ~420 cm^{-1}, meaning the enhanced stiffness of Zn–N bonds upon eIm doping, i.e., restricted flexibility of ZIF-8 [18,40]. Since the ethyl group in eIm exhibits greater electron donating ability than the methyl group in mIm, the Zn–N bond distance with eIm is expected shorter and mechanically stiffer than that with mIm. The restricted flip-flopping motion of eIm-doped ZIF-8 with incorporation of eIm linkers is expected to reduce the effective aperture size of eIm-doped ZIF-8 [40]. On the other hand, as shown in Fig. 6, the first gate-opening pressure decreased with higher eIm contents, indicating that eIm-doped ZIF-8 might possess more open micropore structure (i.e., larger aperture) of eIm-doped ZIF-8 and/or more favorable interaction with adsorbates than ZIF-8 [39]. The more open micropore is likely due to the reconfiguration of the aperture structure resulting from the presence of bulkier eIm linkers while the more favorable interaction with adsorbates might be owing to the bulkier ethyl groups. The slight increase in the C_3H_6 permeability of the PI/eIm$_{0.2}$-ZIF-8 compared to that of the PI/ZIF-8 might be attributed mostly to the change in the microstructure, not much to do with eIm doping since the actual dopant concentration (~7%) is much less than a percolation threshold [37]. As the dopant concentration further increases as in the case of the PI/eIm$_{0.4}$-ZIF-8 and PI/eIm$_{0.6}$-ZIF-8, the significantly enhanced C_3H_6/C_3H_8 separation factors of the PI/eIm-doped ZIF-8 MMMs were observed, which were attributed likely to the reduced effective aperture size of the eIm-doped ZIF-8.

As comparison, we prepared PI/eIm-doped ZIF-8 MMMs using conventional physical blending method. Fig. 7 and Table S2 compare their C3 separation performances with those by PMMOF. Comparing with the MMMs by PMMOF, the PI/eIm-doped ZIF-8 MMMs prepared by blending method showed higher permeabilities and lower C_3H_6/C_3H_8 separation factors, which might come from the relatively poor adhesion between polymer and filler (Fig. S11). The poor adhesion between eIm-doped ZIF-8 and polymer matrix possibly might be owing to the eIm concentration as well as the increased particle size with increasing eIm contents. This denotes that the PMMOF is more effective in obtaining enhanced MMM microstructures (i.e., interfacial structures, filler dispersion, etc.). The PI/ZIF-8 by PMMOF exhibited decreased propylene permeability than the PI/ZIF-8 prepared by blending method, likely due to the densification of polymer upon PMMOF (i.e., reduced polymer free volume upon *in-situ* growing ZIF fillers) [23]. The densification of polymer upon PMMOF might also play a role in enhancing the separation factors.

3.3. eIm-doped ZIF-8-based mixed-matrix hollow fiber membranes

For large-scale commercial gas separation applications, hollow fiber membranes are preferred than flat sheet membranes [6,41]. As a proof-of-concept, the eIm-doping strategy combined with PMMOF was applied on scalable hollow fiber membranes (HFMs). Thin and selective 6FDA-DAM layers were coated with thicknesses of ~1 μm on porous PES hollow fibers (Fig. 8a). The PI coating layers were transformed to PI/ZIF-8 (Fig. 8b) or PI/eIm$_{0.6}$-ZIF-8 (Fig. 8c) layers while maintaining membrane thickness. The formation of ZIF-8 and eIm-doped ZIF-8 was confirmed by X-ray diffraction (Fig. 8d). Comparing with the PI/ZIF-8

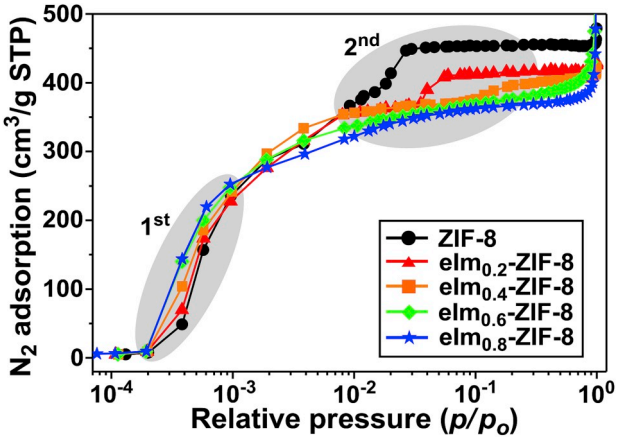

Fig. 6. N_2 adsorption isotherms of ZIF-8 and eIm-doped ZIF-8 at 77 K with log scale abscissa plot.

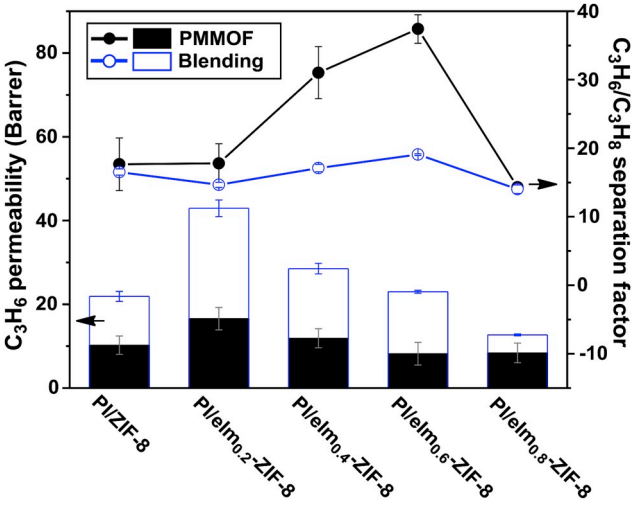

Fig. 7. Comparison of C_3H_6/C_3H_8 separation performance of PI/eIm-doped ZIF-8 MMMs prepared by PMMOF and a conventional blending method.

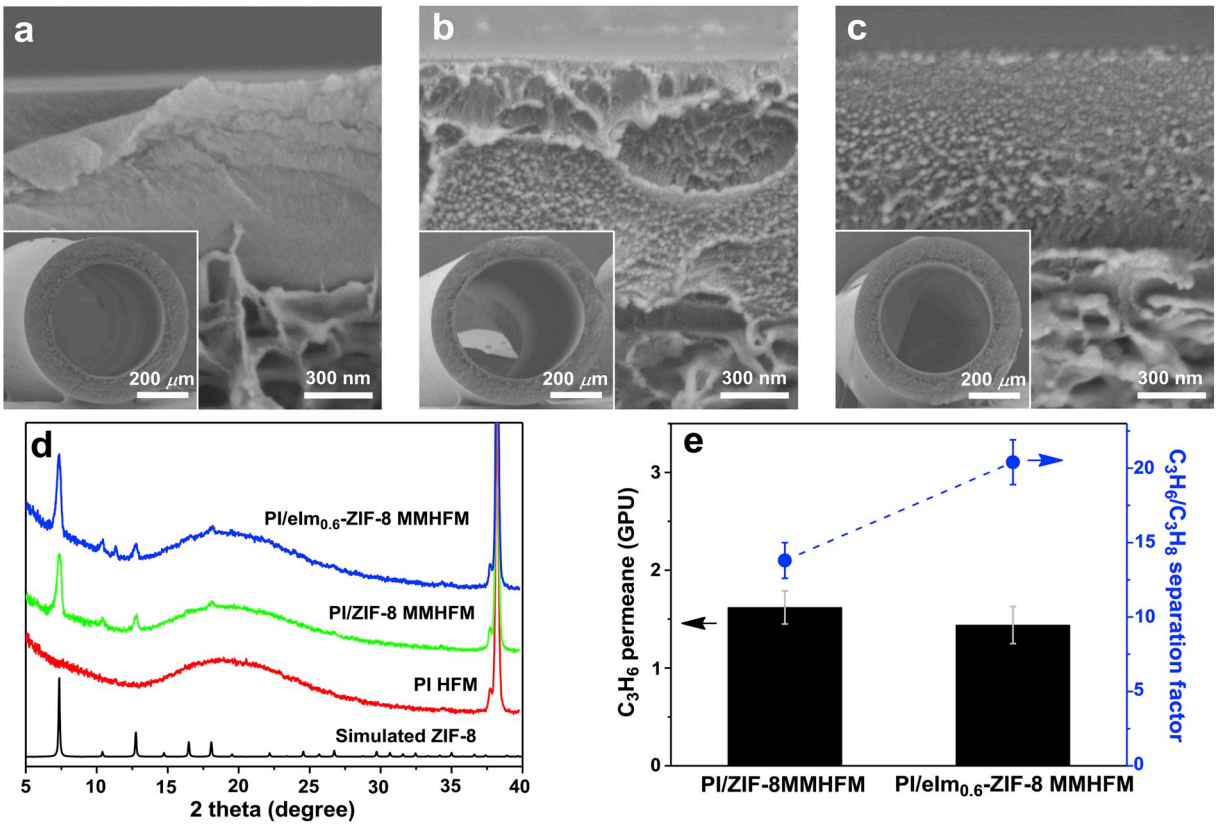

Fig. 8. **a-c** SEM images of PI HFM (a), PI/ZIF-8 MMHFM (b), and PI/eIm$_{0.6}$-ZIF-8 MMHFM (c). **d** XRD diffraction patterns of PI HFM and PI/ZIF MMHFMs. **e** C_3H_6/C_3H_8 separation performance of PI/ZIF-8 and PI/eIm$_{0.6}$-ZIF-8 MMHFMs.

mixed-matrix hollow fiber membranes (MMHFMs), the PI/eIm-doped ZIF-8 MMHFMs showed the improved C_3H_6/C_3H_8 separation factor and comparable C_3H_6 permeance (Fig. 5e), which is consistent with the results of flat membranes.

4. Conclusions

Here, we reported, for the first time, a linker doping strategy as a novel means to improve gas separation performances of MMMs. 2-ethylimidazole (eIm) was used as a dopant ligand to tune the effective aperture size of ZIF-8 filler in MMMs. eIm-doped ZIF-8 fillers with the dopant content as high as 50 mol% were successfully formed *in-situ* in MMMs using the PMMOF process. The eIm-doped ZIF-8 containing MMMs with a relatively low eIm content (7 mol%) enlarged the pore structure of ZIF-8, enhancing C_3H_6 permeability (~62%) while maintaining C3 separation factor as compared with ZIF-8 containing MMMs. On the contrary, at the relatively high eIm content (~31 mol%), the eIm-doped ZIF-8 in MMMs dramatically improved the C3 separation factor (~111%) with a small decrease in the propylene permeability despite the slightly low filler contents. The improvement in the C3 separation factor was attributed to the restricted flip-flopping motion of ZIF-8, thereby reduced the effective aperture size of ZIF-8 owing to the presence of bulkier eIm in the framework. Finally, the linker doping strategy along with the *in-situ* MOF formation based MMM fabrication strategy (PMMOF) was successfully applied to prepare eIm-doped ZIF-8-containing mixed-marix hollow fiber membranes, showing enhanced C3 separation factor as compared with those MMMs containing undoped ZIF-8. The ability to tune the molecular sieving properties of ZIF-8 fillers in MMMs combined with the capability of producing MMHFMs with sub-micron thick selective layers is expected a major step toward the scalable applications of high-performance MMMs for gas separations.

Acknowledgement

H.-K.J. acknowledges the financial support from the National Science Foundation (CBET-1510530). This publication was made possible in part by NPRP grant # 8-001-2-001 from the Qatar National Research Fund (a member of Qatar Foundation). The findings achieved herein are solely the responsibility of the authors. The National Science Foundation supported the FE-SEM acquisition under Grant DBI-0116835, the VP for Research Office, and the Texas A&M Engineering Experimental Station. The authors would like to thank Dr. Micah Green and Mr. Xiaofei Zhao in Chemical Engineering at Texas A&M University for the use of TGA.

Appendix A. Supplementary data

Supplementary data to this article can be found online at https://doi.org/10.1016/j.memsci.2019.117689.

References

[1] H.R. Amedi, M. Aghajani, Economic estimation of various membranes and distillation for propylene and propane separation, Ind. Eng. Chem. Res. 57 (2018) 4366–4376.
[2] D.S. Sholl, R.P. Lively, Seven chemical separations to change the world, Nature 532 (2016) 435–437.
[3] W.J. Koros, C. Zhang, Materials for next-generation molecularly selective synthetic membranes, Nat. Mater. 16 (2017) 289–297.
[4] C. Zhang, R.P. Lively, K. Zhang, J.R. Johnson, O. Karvan, W.J. Koros, Unexpected molecular sieving properties of zeolitic imidazolate framework-8, J. Phys. Chem. Lett. 3 (2012) 2130–2134.
[5] C. Zhang, Y. Dai, J.R. Johnson, O. Karvan, W.J. Koros, High performance ZIF-8/6FDA-DAM mixed matrix membrane for propylene/propane separations, J. Membr. Sci. 389 (2012) 34–42.
[6] C. Zhang, K. Zhang, L.R. Xu, Y. Labreche, B. Kraftschik, W.J. Koros, Highly scalable ZIF-based mixed-matrix hollow fiber membranes for advanced hydrocarbon separations, AIChE J. 60 (2014) 2625–2635.

[7] G.A.H. Craig, W. Colling, John V. Bartels, Processes using solid perm-selective membranes in multiple groups for simultaneous recovery of specified products from a fluid mixture, 2004. US.
[8] A. Phan, C.J. Doonan, F.J. Uribe-Romo, C.B. Knobler, M. O'Keeffe, O.M. Yaghi, Synthesis, structure, and carbon dioxide capture properties of zeolitic imidazolate frameworks, Acc. Chem. Res. 43 (2010) 58–67.
[9] J.A. Thompson, C.R. Blad, N.A. Brunelli, M.E. Lydon, R.P. Lively, C.W. Jones, S. Nair, Hybrid zeolitic imidazolate frameworks: controlling framework porosity and functionality by mixed-linker synthesis, Chem. Mater. 24 (2012) 1930–1936.
[10] F. Hillman, J.M. Zimmerman, S.M. Paek, M.R.A. Hamid, W.T. Lim, H.K. Jeong, Rapid microwave-assisted synthesis of hybrid zeolitic-imidazolate frameworks with mixed metals and mixed linkers, J. Mater. Chem. 5 (2017) 6090–6099.
[11] P. Krokidas, M. Castier, S. Moncho, D.N. Sredojevic, E.N. Brothers, H.T. Kwon, H. K. Jeong, J.S. Lee, I.G. Economou, ZIF-67 framework: a promising new candidate for propylene/propane separation. Experimental data and molecular simulations, J. Phys. Chem. C 120 (2016) 8116–8124.
[12] P. Krokidas, S. Moncho, E.N. Brothers, M. Castier, I.G. Economou, Tailoring the gas separation efficiency of metal organic framework ZIF-8 through metal substitution: a computational study, Phys. Chem. Chem. Phys. 20 (2018) 4879–4892.
[13] K. Eum, K.C. Jayachandrababu, F. Rashidi, K. Zhang, J. Leisen, S. Graham, R. P. Lively, R.R. Chance, D.S. Sholl, C.W. Jones, S. Nair, Highly tunable molecular sieving and adsorption properties of mixed-linker zeolitic imidazolate frameworks, J. Am. Chem. Soc. 137 (2015) 4191–4197.
[14] F. Hillman, J. Brito, H.K. Jeong, Rapid one-pot microwave synthesis of mixed-linker hybrid zeolitic-imidazolate framework membranes for tunable gas separations, ACS Appl. Mater. Interfaces 10 (2018) 5586–5593.
[15] J. Sanchez-Lainez, A. Veiga, B. Zornoza, S.R.G. Balestra, S. Hamad, A.R. Ruiz-Salvador, S. Calero, C. Tellez, J. Coronas, Tuning the separation properties of zeolitic imidazolate framework core-shell structures via post-synthetic modification, J. Mater. Chem. 5 (2017) 25601–25608.
[16] P. Krokidas, S. Moncho, E.N. Brothers, M. Castier, H.K. Jeong, I.G. Economou, On the efficient separation of gas mixtures with the mixed-linker zeolitic-imidazolate framework-7-8, ACS Appl. Mater. Interfaces 10 (2018) 39631–39644.
[17] Q.Q. Hou, Y. Wu, S. Zhou, Y.Y. Wei, J. Caro, H.H. Wang, Ultra-tuning of the aperture size in stiffened ZIF-8_Cm frameworks with mixed-linker strategy for enhanced CO2/CH4 separation, Angew. Chem. Int. Ed. 58 (2019) 327–331.
[18] F. Hillman, H.K. Jeong, Linker-doped zeolitic imidazolate frameworks (ZIFs) and their ultrathin membranes for tunable gas separations, ACS Appl. Mater. Interfaces 11 (2019) 18377–18385.
[19] M.R.A. Hamid, H.K. Jeong, Recent advances on mixed-matrix membranes for gas separation: opportunities and engineering challenges, Korean J. Chem. Eng. 35 (2018) 1577–1600.
[20] T.S. Chung, L.Y. Jiang, Y. Li, S. Kulprathipanja, Mixed matrix membranes (MMMs) comprising organic polymers with dispersed inorganic fillers for gas separation, Prog. Polym. Sci. 32 (2007) 483–507.
[21] C. Liu, S. Kulprathipanja, A.M.W. Hillock, S. Husain, W. Koros, Recent progress in mixed-matrix membranes, 2008, pp. 787–819.
[22] J.A. Thompson, J.T. Vaughn, N.A. Brunelli, W.J. Koros, C.W. Jones, S. Nair, Mixed-linker zeolitic imidazolate framework mixed-matrix membranes for aggressive CO2 separation from natural gas, Microporous Mesoporous Mater. 192 (2014) 43–51.
[23] S. Park, M.R.A. Hamid, H.K. Jeong, Highly propylene-selective mixed-matrix membranes by in situ metal organic framework formation using a polymer-modification strategy, ACS Appl. Mater. Interfaces 11 (2019) 25949–25957.
[24] S.M. Zhang, A reliable and efficient first principles-based method for predicting pKa values. 4. organic bases, J. Comput. Chem. 33 (2012) 2469–2482.
[25] J. Cravillon, R. Nayuk, S. Springer, A. Feldhoff, K. Huber, M. Wiebcke, Controlling zeolitic imidazolate framework nano- and microcrystal formation: insight into crystal growth by time-resolved in situ static light scattering, Chem. Mater. 23 (2011) 2130–2141.
[26] X.L. Ma, P. Kumar, N. Mittal, A. Khlyustova, P. Daoutidis, K.A. Mkhoyan, M. Tsapatsis, Zeolitic imidazolate framework membranes made by ligand-induced permselectivation, Science 361 (2018) 1008–1011.
[27] R.L. Burns, W.J. Koros, Defining the challenges for C3H6/C3H8 separation using polymeric membranes, J. Membr. Sci. 211 (2003) 299–309.
[28] H.X. Sun, C. Ma, T. Wang, Y.Y. Xu, B.B. Yuan, P. Li, Y. Kong, Preparation and characterization of C60-filled ethyl cellulose mixed-matrix membranes for gas separation of propylene/propane, Chem. Eng. Technol. 37 (2014) 611–619.
[29] B.B. Yuan, H.X. Sun, T. Wang, Y.Y. Xu, P. Li, Y. Kong, Q.J. Niu, Propylene/propane permeation properties of ethyl cellulose (EC) mixed matrix membranes fabricated by incorporation of nanoporous graphene nanosheets, Sci. Rep. 6 (2016).
[30] R.J. Lin, L. Ge, H. Diao, V. Rudolph, Z.H. Zhu, Propylene/propane selective mixed matrix membranes with grape-branched MOF/CNT filler, J. Mater. Chem. 4 (2016) 6084–6090.
[31] H. An, S. Park, H.T. Kwon, H.K. Jeong, J.S. Lee, A new superior competitor for exceptional propylene/propane separations: ZIF-67 containing mixed matrix membranes, J. Membr. Sci. 526 (2017) 367–376.
[32] H.R. Amedi, M. Aghajani, Modified zeolitic-midazolate framework 8/poly(ether-block-amide) mixed-matrix membrane for propylene and propane separation, J. Appl. Polym. Sci. 135 (2018).
[33] F. Yang, H. Mu, C.Q. Wang, L. Xiang, K.X. Yao, L.M. Liu, Y. Yang, Y. Han, Y.S. Li, Y. C. Pan, Morphological map of ZIF-8 crystals with five distinctive shapes: feature of filler in mixed-matrix membranes on C3H6/C3H8 separation, Chem. Mater. 30 (2018) 3467–3473.
[34] X.H. Ma, R.J. Swaidan, Y.G. Wang, C.E. Hsiung, Y. Han, I. Pinnau, Highly compatible hydroxyl-functionalized microporous polyimide-ZIF-8 mixed matrix membranes for energy efficient propylene/propane separation, ACS Appl. Nano Mater. 1 (2018) 3541–3547.
[35] S.H. Kunjattu, V. Ashok, A. Bhaskar, K. Pandare, R. Banerjee, U.K. Kharul, ZIF-8@DBzPBI-BuI composite membranes for olefin/paraffin separation, J. Membr. Sci. 549 (2018) 38–45.
[36] Y. Liu, Z.J. Chen, G.P. Liu, Y. Belmabkhout, K. Adil, M. Eddaoudi, W. Koros, Conformation-controlled molecular sieving effects for membrane-based propylene/propane separation, Adv. Mater. 31 (2019).
[37] R.J. Verploegh, Y. Wu, D.S. Sholl, Lattice-gas modeling of adsorbate diffusion in mixed-linker zeolitic imidazolate frameworks: effect of local imidazolate ordering, Langmuir 33 (2017) 6481–6491.
[38] L. Diestel, N.Y. Wang, B. Schwiedland, F. Steinbach, U. Giese, J. Caro, MOF based MMMs with enhanced selectivity due to hindered linker distortion, J. Membr. Sci. 492 (2015) 181–186.
[39] D. Fairen-Jimenez, S.A. Moggach, M.T. Wharmby, P.A. Wright, S. Parsons, T. Duren, Opening the gate: framework flexibility in ZIF-8 explored by experiments and simulations, J. Am. Chem. Soc. 133 (2011) 8900–8902.
[40] H.T. Kwon, H.K. Jeong, A.S. Lee, H.S. An, J.S. Lee, Heteroepitaxially grown zeolitic imidazolate framework membranes with unprecedented propylene/propane separation performances, J. Am. Chem. Soc. 137 (2015) 12304–12311.
[41] M.J. Lee, M.R.A. Hamid, J. Lee, J.S. Kim, Y.M. Lee, H.K. Jeong, Ultrathin zeolitic-imidazolate framework ZIF-8 membranes on polymeric hollow fibers for propylene/propane separation, J. Membr. Sci. 559 (2018) 28–34.